Materials Advances

ROYAL SOCIETY OF CHEMISTRY

COMMUNICATION

View Article Online
View Journal | View Issue

Check for updates

Cite this: *Mater. Adv.*, 2025, 6, 945

Received 17th December 2024,
Accepted 26th December 2024

DOI: 10.1039/d4ma01262c

rsc.li/materials-advances

Facile tailoring of a multi-element nanocomposite for electrocatalysis†

Mohamed Okasha and Vivek Maheshwari *

Multielement combinations either as high entropy alloys or as nanocomposites are highly effective electrocatalysts for key reactions such as the hydrogen evolution reaction (HER) and the oxygen evolution reaction (OER). Both these reactions are crucial for generation of green hydrogen from water splitting. In this work we demonstrate the concept of using an electrical double layer to modulate the formation of these multielement catalysts. A one-pot, room temperature synthesis method is used to prepare dual functional HER and OER catalysts. The nanocomposite catalyst (NAC) forms chain-like structures composed of Au nanoparticle (AuNP) cores with a shell structure of Pt, Ni, Cu, Co and V that form a combination of metallic and amorphous composite heterostructures on a nanoscale, tailored using the electrical double layer. The NAC achieves low HER and OER overpotentials in 0.1 M KOH with fast kinetics for both reactions.

By combining multiple early transition metals with noble metal catalysts, synergistic effects are observed that can improve water splitting performance. Among such multielement composites are high entropy alloys (HEAs), which are composed of five or more elements.[1–5] While ideally the alloying elements do not need to be precisely equimolar, the term high entropy was rationalized from the hypothesis that when five or more equimolar elements are mixed, the configurational entropy of mixing's contribution to free energy would overcome the enthalpy of forming intermetallic compounds. This would in turn lead to the formation of stable solid solutions over intermetallic compounds.[2] HEAs are an emerging class of catalysts owing to their high structural and thermal stability, a result of their high entropy and sluggish diffusion effects. The lattice distortion and cocktail effects in HEAs provide many unique coordination environments on the catalyst surface that can enhance electrocatalytic activity.[3,6,7] Similar advantages will also be present in nanocomposites that use a combination of elements (5 or more) and hence can provide a multitude of surface sites that can catalyse key reaction steps in processes such as the HER and OER for water electrolysis.[8,9] Both the HER and OER, the two half reactions in water electrolysis, have multiple steps and also involve a variety of intermediate species.[10–12] Sluggish kinetics for either reaction can impede the water splitting process. Also hindering the wide scale application of water electrolysis is the need for either highly acidic or basic environments, as water splitting requires extreme conditions to achieve good kinetics.[13–15] Typically, noble metal catalysts such as Pt, Ir, and Ru which are effective for the HER and OER are used in combination with early transition metals such as Ni, Cu, Co, Fe and V for developing such multi-element combinations to further improve the performance and stability.[1,10,16–18]

Synthesizing HEAs and such nanocomposites using either a bottom-up or a top-down approach can involve wet chemistry and high temperature methods and can be lengthy, adding to the cost of the catalyst.[6,13] These methods typically also have little control over the distribution of the elements and their oxidation states. Herein, we show the concept of using a colloidal template and its electrical double layer (EDL) to direct the synthesis of a bifunctional water splitting nanocomposite catalyst (NAC). The one-pot method is easy and conducted at room temperature. The developed catalyst consists of Au nanoparticle (AuNP) chains as a template structure with a surface shell layer composed of a PtNiCuCoV mixture. The NAC structure results from the use of the EDL on the AuNP chains to direct the synthesis.[19] As a concept, we show that this EDL directed synthesis results in key differences in the NAC structure compared to undirected synthesis. The Au–PtNiCuCoV catalyst exhibits, as a result of these structural changes, exceptional HER and OER performances under weak alkaline conditions with good kinetics.

The NAC is prepared through self-assembly of 10–12 nm AuNPs into distributed chain-like structures in aqueous media using metal cations of Pt^{4+}, Ni^{2+}, Cu^{2+}, Co^{2+}, and V^{3+}. These metal cations interact preferentially with the negatively charged AuNPs through the EDL causing chain-like structures to form.

Department of Chemistry, The Waterloo Institute for Nanotechnology, University of Waterloo, 200 University Av. W., Waterloo, ON, N2L 3G1, Canada.
E-mail: vmaheshw@uwaterloo.ca

† Electronic supplementary information (ESI) available. See DOI: https://doi.org/10.1039/d4ma01262c

Open Access Article. Published on 27 December 2024. Downloaded on 2/2/2026 12:09:34 PM. This article is licensed under a Creative Commons Attribution-NonCommercial 3.0 Unported Licence.

Open Access Article. Published on 27 December 2024. Downloaded on 2/2/2026 12:09:34 PM.
This article is licensed under a Creative Commons Attribution-NonCommercial 3.0 Unported Licence.

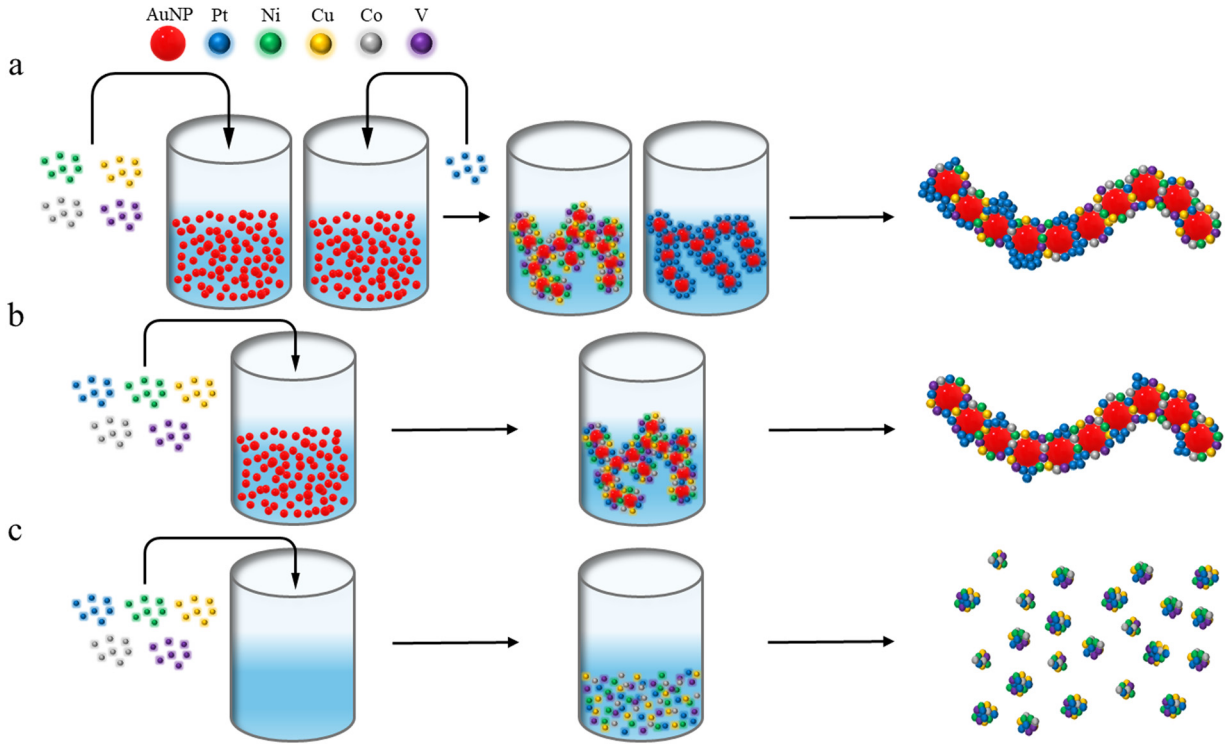

Scheme 1 Schematic illustration outlining how different preparation methods can lead to structural changes on the NAC. (a) Au chains are self-assembled separately with Pt^{4+} cations and the transition metal cations (V^{3+}, Co^{2+}, Cu^{2+}, and Ni^{2+}). The chains are then mixed and subsequently reduced to form the NAC mixed chains. (b) All the five cations are simultaneously added to the AuNP solution for self-assembly and then reduced. This leads to the formation of NAC mixed ions. (c) A control is made without the use of AuNPs as a chain template, where the five cations are added to a solution (just water) and then reduced leading to the formation of NACs in H_2O.

The AuNP and metal cation mixture is then reduced to form the NAC. Depending on how the metal cations are added to the AuNPs, the atomic distribution can be altered.[19,20] Scheme 1 shows how the distribution of atoms on the AuNP surface changes when AuNP Pt^{4+} chains and AuNP Ni^{2+}, Cu^{2+}, Co^{2+}, V^{3+}chains are separately prepared and then mixed together (NAC mixed chains) (Scheme 1a) *versus* simultaneously mixing all metal salts at the same time (NAC mixed ions) (Scheme 1b). Adding all metal cations at the same time to the AuNPs results in a more homogenous distribution of atoms after reduction. This is evident from TEM observations, which show small Pt nanoparticles evenly distributed on the AuNP surface (Fig. 1a). More isolated domains of Pt nanoparticles form on the AuNP surface when the chains are prepared separately and then mixed (Fig. 1b) and as a result not as evenly distributed. Differences are also observed in other elements, as will be discussed later. Both preparation methods resulted in chain-like structures with AuNP cores and a heterogenous mixture of Pt, Ni, Cu, Co and V forming a shell on the AuNP surface. An amorphous layer is also observed surrounding the AuNP chains (Fig. 1c) and metallic–metallic and metallic–amorphous interfaces can be observed in these NACs (Fig. 1c inset). Electron energy loss spectroscopy (EELS) for the NAC mixed ions further confirms the formation of the heterogenous composite on the AuNP shell (Fig. 1d–j). Pt, Cu and V can be observed directly on the AuNP surface. While Ni and Co are observed more on the diffuse layer around the AuNP surface, which corresponds to the amorphous layer surrounding the NAC. Mixing the metal cations in water without the use of AuNPs resulted in the formation of a nanocomposite lacking the chain-like structure and its heterogeneity (Scheme 1c and Fig. S1, ESI†). Inductively coupled plasma mass spectroscopy (ICP-MS) shows that the relative atomic distributions of elements in the NAC mixed ions are 72.8, 1.4, 16.8, 1.2 and 7.8 at% for Pt, Ni, Cu, Co, and V, respectively. This demonstrates that the NAC is primarily a Pt composite with high concentrations of Cu and V and low concentrations of Ni and Co. The NAC mixed chains also show a similar composition (75, 1.5, 12.8, 0.3, and 10.2 at%), while the NAC made without AuNPs shows a more homogenous atomic distribution (29.8, 12.8, 30, 10.6, and 16.7 at%).

The difference in the composition and distribution is also because of the Au nanoparticles (zeta potential of ~ -35 mV) whose EDL leads to the preferential accumulation of the Pt^{4+} ions (and V^{3+}) compared to the divalent ions.[21] This is due to the concentration of the ions in the EDL being exponentially dependent on their charge. The higher concentration of Cu is due to its ability to form intermetallics with Pt at very low concentrations compared to other transition metals.[22–24] Meanwhile, in the synthesis without the use of the AuNP chain template, purely entropic considerations lead to a more uniform distribution of the five elements. The chain like morphology of the NAC is also confirmed by UV-vis absorption spectroscopy

© 2025 The Author(s). Published by the Royal Society of Chemistry

Open Access Article. Published on 27 December 2024. Downloaded on 2/2/2026 12:09:34 PM.
This article is licensed under a Creative Commons Attribution-NonCommercial 3.0 Unported Licence.

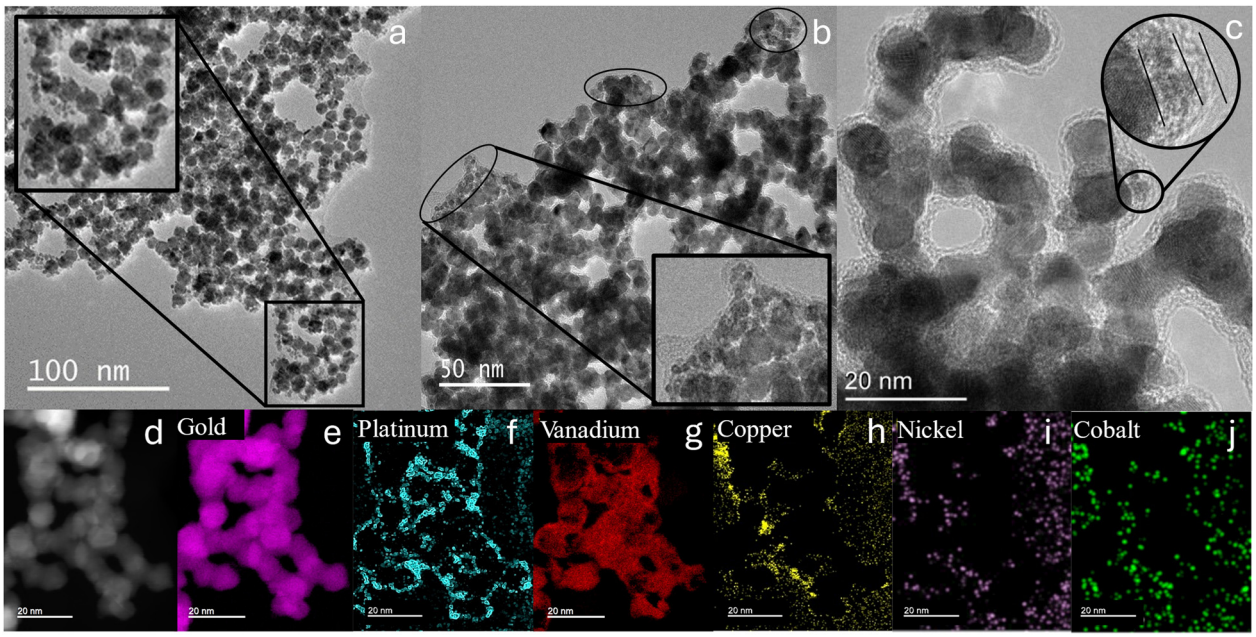

Fig. 1 Structural characterization using TEM and EELS for the NAC. (a) TEM image of NAC mixed ions outlining the chain-like structure and even distribution of Pt nanoparticles on the surface (inset image). (b) TEM image of NAC mixed chains outlining regions of high (circled) and low-density Pt domains. (c) HRTEM image of NAC mixed ion showing the presence of crystalline and amorphous domains. Clearly seen in the higher magnification image of the inset is that next to the AuNP is a crystalline–crystalline interface and then a crystalline–amorphous interface. The annular dark field (d) and EELS spectrum (e)–(j) of Au, Pt, V, Cu, Ni and Co showcasing the atomic spatial distribution on the NAC mixed ion surface.

(Fig. S2, ESI†) where Au nanoparticles show a typical plasmon resonance peak at ~525 nm. In contrast, for the NACs prepared with the AuNP chain like template, this red shifted to ~620–640 nm due to the delocalization of the plasmon on the chain.

Grazing incidence X-ray diffraction (GIXRD) data (Fig. S3, ESI†) for both the NAC mixed ions and mixed chains primarily showed crystalline Pt peaks, shifted to lower 2θ angles indicating a distortion in the crystal lattice of Pt. For example, Pt (220) peaks shifted from 67.55° (for Au–Pt) to 65.25° for both NAC mixed ions and mixed chains. No other prominent peaks were observed from any of the other transition metals either due to their low concentration on the surface or due to the formation of the amorphous phase. In contrast, for the NACs made without the AuNP chain like template, a contraction in the Pt lattice was observed. The Pt (220) peak, for *e.g.*, shifts to a higher 2θ angle of 69.65°. The peaks are also broad, which further indicates the small size of the crystalline domains. Some alloy formation and overlap in XRD peaks with Au cannot be ruled out. The effect of both lattice shrinkage and expansion can lead to enhanced HER and OER activity.[25–27] The difference in the strains between the templated and untemplated NACs indicates a fundamental difference in their formation mechanism. Specifically, the EDL directed synthesis alters the chemical composition of the NACs, which results in the observed differences. The difference in chemical composition will be further discussed below based on X-ray photoelectron spectroscopy (XPS) results.

XPS analysis was conducted to further detail the differences in the samples. XPS data (Fig. 2) show that Pt 4f peaks on both NAC mixed chains and NAC mixed ions (Fig. 2a) lack shoulders that are observed at higher binding energies (72 and 78 eV) on the NAC without AuNPs. This indicates that NAC samples prepared in the presence of AuNPs contain relatively less amounts of Pt^{2+}. The higher binding energies of the Pt peaks are also an indication of electron transfer to neighbouring atoms on the catalyst surface in both Au chain templated NACs.[28] This indicates that the Pt atoms interact with other atoms (Ni, Cu, Co and V) confirming a distorted lattice which was observed in GIXRD (Fig. S3, ESI†).

Another critical observation is that the presence of metallic species for the transition metals Ni, V, Cu and Co is predominantly observed for NACs made with the Au chain template. This can be clearly observed in the case of Ni (Fig. 2b), where only the NAC mixed chain and NAC mixed ion samples show a metallic Ni peak (813 eV). This peak is absent in samples that lacked either the Au chain template or Pt. Similarly, for V, a long tail observed in the low energy region for NAC mixed chains and mixed ions shows the presence of metallic 'V'. This is absent for the other NAC samples made without the Au chain template or Pt. XPS peak analysis (Table S1, ESI†) shows that in all cases the NAC mixed chains and mixed ion samples have a higher fraction of transition metals in a metallic form compared to the samples made without the Au chain template or without Pt. This leads us to conclude that stable multielement metallic compounds are only prepared in the presence of a high fraction of Pt. This is possible only when the NACs are prepared with the Au chain template in the presence of Pt^{4+}. The preferential accumulation of the Pt^{4+} ions in the EDL (due to their high charge) of the Au chains leads to the formation of NACs with a high fraction of Pt and hence also inclusion of metallic species of Co, Cu, Ni and V. In the absence of the Au

Open Access Article. Published on 27 December 2024. Downloaded on 2/2/2026 12:09:34 PM.
This article is licensed under a Creative Commons Attribution-NonCommercial 3.0 Unported Licence.

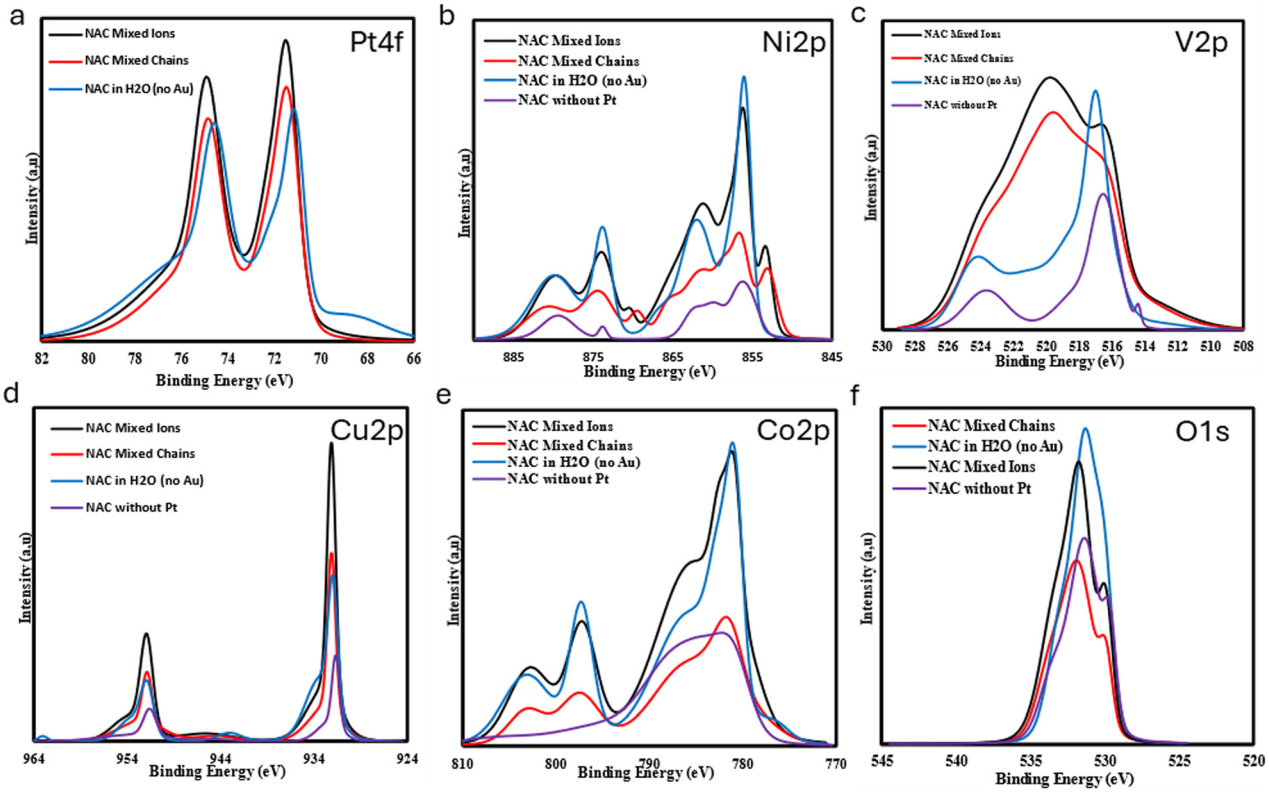

Fig. 2 XPS characterization of NAC mixed ions, NACs, mixed chains, NACs in H_2O, and NACs without Pt, for the main elements: (a) Pt 4f, (b) Ni 2p, (c) V 2p, (d) Cu 2p, (e) Co 2p and (f) O 1s.

chain template, the NAC is formed with a lower fraction of Pt which limits the formation and inclusion of the transition metals in the metallic form.

Furthermore, in the NAC mixed chains and NAC mixed ion samples, besides the metallic form, higher oxidation states of the transition metals are also observed. For example, larger shoulders were observed at 858 eV (Fig. 2b) corresponding to a greater presence of oxidized Ni^{3+} on the catalyst surface in the case of NACs made with the Au template. This catalytically active form of Ni is beneficial for both the HER and the OER.[29–31] V is one of the elements found in high concentrations on the NAC surface and observing V 2p peaks in Fig. 2c shows that, in the absence of Au or Pt, the primary peak observed is that of V^{3+} (517 eV). Meanwhile, on both the Au chain templated and Pt containing NACs, the larger and broader spectra observed (518–524 eV) correspond to an increased presence of both V^{4+} and V^{5+} on the NAC catalysts, and peak fitting indicated that V^{4+} was more prominent in the NAC mixed ions. A mixture of metallic Cu, Cu^{1+} and Cu^{2+} was likely present in all samples (Fig. 2d), but the NAC mixed ion contained relatively more Cu^{2+} than the NAC mixed chain sample (937 eV). The highly oxidized surface of the NACs was also prominent on both Co 2p (Fig. 2e) and O 1s (Fig. 2f) spectra. The NACs likely contain a mixture of Co^{1+}, Co^{2+}, and Co^{3+}; however, the multiplet peak present on the NAC mixed ions (fitted at 781 and 782.5 eV) and the larger shoulder at higher energies indicate a larger presence of Co^{3+}. The O 1s spectra demonstrated that the NAC mixed ions contained the most hydroxides as it had the widest shoulder (533 eV) due to the formation of metal hydroxides on the catalyst surface.

Overall, XPS data showed that the surface of the NAC catalysts, in particular the NAC mixed ions, was highly oxidized and contained a wide range of oxidation states for each of its corresponding transition metals. The presence of oxides and oxyhydroxides on the catalyst surface can greatly enhance the OER and HER catalytic ability of a catalyst in alkaline media as demonstrated in the literature and later on in this work.[29–31] XPS also confirmed the presence of metallic elements (Ni, V, Cu and Co) in NACs (especially in mixed ion and mixed chain catalysts), implying that there is crystalline composite formation with Pt which will distort the Pt lattice as confirmed by XRD. Some alloy formation with Au cannot be ruled out; however, the shift in the Au 4f spectra is small (Fig. S4, ESI†). The mixed ion and mixed chain NAC surfaces therefore likely consist of a cocktail of Pt-rich crystalline regions interfacing with the surrounding amorphous regions (Fig. 1c), which are composed of metallic oxides/hydroxides.

The metallic and amorphous regions on the surface of the NAC should provide a multitude of potential catalytic sites for the HER and the OER making it a suitable multifunctional catalyst.[32–35] Therefore, HER and OER performances were tested in 0.1 M and 0.5 M KOH solutions, and the polarization and Tafel curves are shown in Fig. 3. In 0.1 M KOH, the NAC mixed ions and the NAC mixed chains showed the best overpotential for the HER. The NAC mixed ion catalyst showed the

© 2025 The Author(s). Published by the Royal Society of Chemistry

Open Access Article. Published on 27 December 2024. Downloaded on 2/2/2026 12:09:34 PM.
This article is licensed under a Creative Commons Attribution-NonCommercial 3.0 Unported Licence.

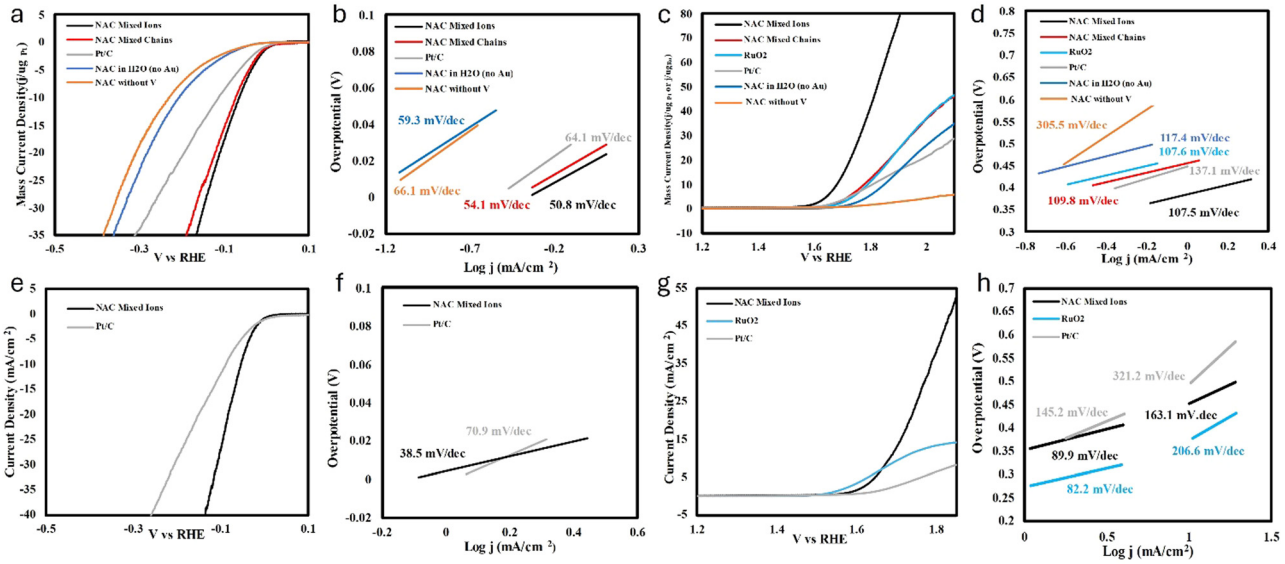

Fig. 3 Polarization curves and Tafel slopes for NACs in 0.1 M KOH (a)–(d) and 0.5 M KOH (e)–(h). (a) HER polarization curves and (b) their respective Tafel slopes for various NACs in 0.1 M KOH. (c) OER polarization curves and (d) their respective Tafel slopes for various NACs in 0.1 M KOH. (e) HER polarization curves and (f) Tafel slopes for NAC mixed ions and Pt/C in 0.5 M KOH. (g) OER polarization curves and (h) Tafel slopes for NAC mixed ions, RuO_2 and Pt/C in 0.5 M KOH.

best performance with an overpotential of 91 mV at 10 mA cm^{-2}, compared to 20% Pt/C which had an overpotential of 189 mV at 10 mA cm^{-2} (Fig. 3a). RuO_2, which is a catalyst for the OER, as expected showed limited capacity for the HER with an overpotential of 350 mV at 10 mA cm^{-2} (Fig. S5, ESI†). The NAC mixed ion catalyst also had the best kinetics with a Tafel slope of 50.8 mV dec^{-1} (Fig. 3b) and the highest mass activity of 0.773 mA μg_{Pt}^{-1} at 70 mV and 1.24 mA μg_{Pt}^{-1} at 100 mV, which is $\sim$ twice that of Pt/C. The NAC mixed ion catalyst slightly outperformed the NAC mixed chain catalyst, which can be attributed to the difference in spatial distribution on the catalyst surface, implying that the even distribution of Pt and the transition metals on the surface was a contributing factor to the increase in HER performance. As a control, the NAC made without the use of AuNPs as a chain template was also tested (NAC in H_2O) and it showed considerably worse HER performance (Fig. 3a and b). This demonstrates the importance of the EDL in directing the NAC formation process. The resulting core–shell chain-like structure of the NAC also exposes more surface-active catalytic sites and increases the electron transport and mass activity, improving reaction kinetics.

The presence of 'V' in the catalyst was essential, as the NAC prepared without 'V' (substituted with Fe^{2+}) showed poor HER performance (Fig. 3a and b). This implies that V in the NAC played a major role in the HER mechanism. Pt on the NAC surface still played the largest role for the HER as the NAC without Pt undergoes the HER at extremely large overpotentials (Fig. S6, ESI†).

The bifunctionality of the NAC mixed ions is shown by its ability for the OER in 0.1 M KOH. Polarization and Tafel curves (Fig. 3c and d) for the NAC mixed ion catalyst showed an overpotential of 523 mV at 10 mA cm^{-2} with a Tafel slope of 107.5 mV dec^{-1}. In comparison, RuO_2 had an overpotential of 671 mV at 10 mA cm^{-2} and a Tafel slope of 107.6 mV dec^{-1}. The NAC mixed ions also showed the best kinetics as the gap in OER performance increased at higher overpotentials relative to RuO_2. The other NACs also start saturating at higher overpotentials. This is also reflected in mass activity (based on the noble metal Pt/Ru mass), for example, at an overpotential of 570 mV the NAC mixed ions have a value of 30 A mg_{Pt}^{-1} and that of Ru_2O is only at 7.7 A mg_{Ru}^{-1}.

The NAC mixed chains performed considerably worse for the OER, implying that the even distribution of elements on the NAC surface plays a crucial role in the formation of the catalytic active sites for the OER (in comparison to the HER). The EDL directed NAC formation, and the presence of 'V' was also shown to be key for the improved OER performance (Fig. 3c and d). The OER is generally known to have sluggish kinetics, primarily due to the multitude of steps involved from adsorption, deprotonation of water, then the coupling of oxygen intermediates, followed by desorption.[11,36] OER kinetics can be improved by optimizing *d*-spacings and also through inducing strain by lattice expansion.[25–27] In the NAC mixed ions, both these factors will be observed, as seen from the XRD results and the formation the of multi-element composites that will alter the local energy structure of the binding sites.[5,37]

To compare the NAC's performance with other HER and OER catalysts, it was tested in 0.5 M KOH. The NAC mixed ion catalyst showed better HER performance with a lower overpotential of 54.5 mV at 10 mA cm^{-2} *vs.* 70 mV for 20% Pt/C (Fig. 3e). It also had significantly faster kinetics (Fig. 3f) with a Tafel slope of 38.5 mV dec^{-1} (*vs.* 70.9 mV dec^{-1} for 20% Pt/C). The OER overpotential for NAC mixed ions improved in 0.5 M KOH to 453 mV at 10 mA cm^{-2} with a Tafel slope of 89.9 mV dec^{-1}. RuO_2 overpotentials and kinetics also improved, where its performance and kinetics are comparable at low overpotentials to the NACs. However, at higher overpotentials, the NAC outperforms RuO_2 as

Open Access Article. Published on 27 December 2024. Downloaded on 2/2/2026 12:09:34 PM.
This article is licensed under a Creative Commons Attribution-NonCommercial 3.0 Unported Licence.

it probably starts running into transport limitations (Fig. 3g and h) which leads to significantly higher Tafel slopes (Fig. 3h). The NAC mixed ions were also tested in 0.5 M H_2SO_4, and the overpotential was found to be 33 mV at 10 mA cm^{-2}, comparable to other Pt based alloys (Fig. S7, ESI†).

The close values of the Tafel slopes in the HER for the NAC catalyst and Pt/C show that they have similar rate limiting steps.[38] However, the lower overpotential for the NAC mixed ion catalyst illustrates its faster kinetics. In the case of the OER, the NAC catalysts have a similar Tafel slope as RuO_2 (and much lower than Pt/C) which may imply the same rate limiting step.[38] However again, the NAC mixed ion catalyst has faster kinetics than RuO_2. This illustrates that the NAC catalysts does provide a heterogeneity in surface sites, where both the facile HER (similar to Pt/C) and the facile OER (similar to RuO_2) is possible. The NACs made by the EDL directed synthesis showed significantly better performance (especially mixed ions). This illustrates that the formation of a heterogenous structure with close proximity between nanoscale domains of the multielement metallic Pt composite and the amorphous composite with transition metal oxides and hydroxides is required for achieving the bifunctional behaviour with fast kinetics. The electrochemical impedance spectroscopy (EIS) results for the NAC catalysts (Fig. S8, ESI†) show that both the NAC mixed ions and mixed chains, as well as Pt/C, demonstrated good electron transport kinetics with the exception of the NAC in H_2O. The catalysts had relatively similar R_{CT} at around 8–9 Ω with smaller semi-circles compared to the NAC in H_2O, which had a significantly larger semi-circle and R_{CT} of around 250 Ω. This further demonstrated the significance of the AuNP template as an electron transport material for the NAC catalysts.

The NAC's improved water splitting performance is attributed to more optimal hydroxide and proton adsorption/desorption on the catalyst surface, both of which are key descriptors for HER and OER performance.[6,14,39] Cyclic voltammetry (CV) for hydrogen underpotential adsorption/desorption in 0.1 M KOH (Fig. 4) was performed for the catalysts. The NAC mixed ions (Fig. 4a) demonstrated a higher potential for H adsorption, E^{H}_{ads} (a broad peak from 0.211 V to 0.261 V), as well as a lower potential for H desorption, E^{H}_{des} (a broad peak centred at 0.261 V) making $\Delta E = E^{H}_{des} - E^{H}_{ads}$ for NAC mixed ions very small (overlapping peak regions). In comparison, Pt/C has an E^{H}_{ads} peak at 0.2 V and an E^{H}_{des} at 0.321 V, leading to an ΔE of ~0.121 V. Au–Pt chains (with no use of transition metals) have an E^{H}_{ads} peak at 0.241 V and E^{H}_{des} peak at 0.281 V, leading to an ΔE of ~0.04 V. This signifies that NAC mixed ions have the lowest barrier for the HER. Furthermore, both peaks are broad in the NAC sample signifying its variety of surface sites for H-interaction. The OH^- adsorption and desorption are also crucial steps for the HER and the OER. We observe that, for NAC mixed ions, Pt/C and Au–Pt catalyst, critical differences are observed in hydroxide adsorption and desorption (Fig. 4a). For the NAC mixed ions, the OH^-adsorption E^{OH}_{ads} starts at ~0.731 V with a peak observed at 0.951 V. For Pt/C, these values are 0.731 V and 0.841 V, and for Au–Pt chains, these values are 0.731 V and 0.811 V. Meanwhile, OH-desorption E^{OH}_{des} is observed in NAC mixed ions with a broad peak from 0.801 to 0.691 V. In contrast, Pt/C and Au–Pt show relatively sharp E^{OH}_{des} peaks at 0.581 V and 0.641 V, respectively. The NAC mixed ion sample has an overlap in potential between E^{OH}_{ads} and E^{OH}_{des}, signifying its relative ease in comparison to the Pt/C and Au–Pt samples. Furthermore, the peaks are very broad in the NAC mixed ion sample which arises from its heterogeneity in surface sites that interact and lead to OH^- adsorption and desorption over a broader potential range.[40] Likewise, the NAC mixed chains also showed similar adsorption/desorption profiles (Fig. 3b), but the NAC without V or Pt and without AuNPs (NAC in H_2O) did not show prominent H nor OH^- adsorption/desorption peaks. The TEM images of the NAC in H_2O (Fig. S1, ESI†) confirm their size of ~4–5 nm and hence surface area effects are not a factor. These results further

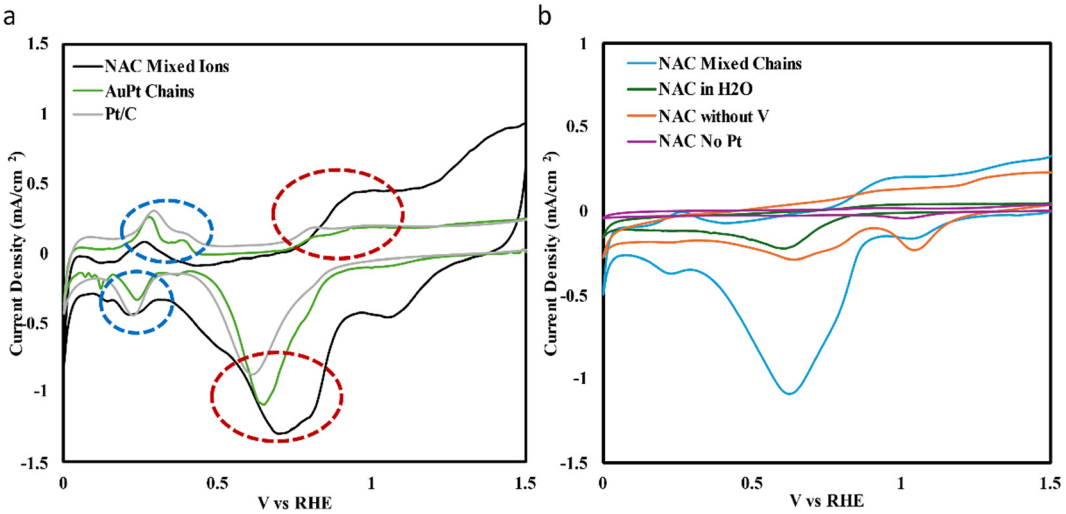

Fig. 4 CVs of catalyst samples in 0.1 M KOH showing the H-adsorption and desorption regions (dashed circles in blue) and the OH-adsorption and desorption regions (dashed circles in red) for (a) NAC mixed ions, AuPt chains and Pt/C and (b) NAC mixed chains, NAC in H_2O, NAC without vanadium and NAC with no platinum.

© 2025 The Author(s). Published by the Royal Society of Chemistry

Open Access Article. Published on 27 December 2024. Downloaded on 2/2/2026 12:09:34 PM.
This article is licensed under a Creative Commons Attribution-NonCommercial 3.0 Unported Licence.

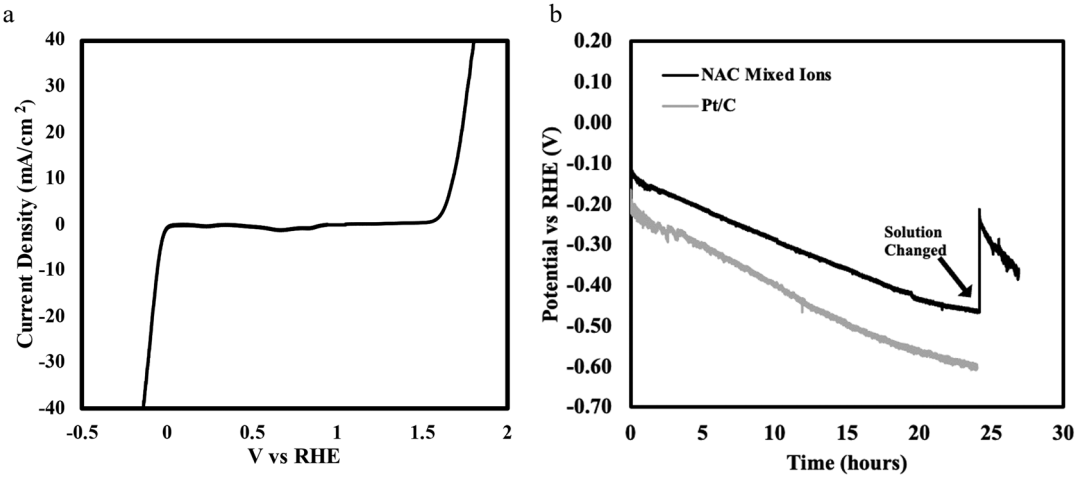

Fig. 5 Demonstration of NAC mixed ion multifunctional water splitting and stability performance. (a) Polarization curve of NAC mixed ions in 0.5M KOH demonstrating multi-functional water splitting with ability to sustain high current densities. (b) Chronopotentiometry 24-hour stability test for NAC mixed ions and 20% Pt/C in 0.1 M KOH, where the NAC demonstrated more stable performance and ability to recover catalytic activity.

confirm that the NAC mixed ions provide a unique heterogenous surface compared to the other materials which is key to their electrocatalytic activity for both the HER and the OER.

Overall, this work demonstrated that the spatial distribution of elements on the catalyst surface as directed by the EDL can have a significant effect on HER and OER performance. A homogenous distribution of Pt on the AuNP chain surface is essential for Pt to form a stable composite with other elements in their elemental state. This is coupled with regions of transition metal oxides and hydroxides. The NAC mixed ion catalyst specifically has a more homogenous distribution of these regions leading to its multifunctional ability for both the HER and the OER. We also observe that without the EDL directed synthesis (NAC in H_2O) the catalyst does not show such structural heterogeneity and hence is a poor catalyst for the HER and the OER.

Conclusions

This work demonstrated an easy and quick method to synthesize a multi-element PtNiCuCoV NAC with good HER and OER catalytic activity under weak alkaline conditions. Both water splitting reactions can be observed with good kinetics (Fig. 5a) for the NAC mixed ions at high current densities with low overpotentials. Furthermore, the NAC mixed ion catalyst also demonstrated stable performance towards the HER (Fig. 5b) over a 24-hour period. Chronopotentiometry (at 10 mA cm^{-2}) showed that the NAC mixed ion overpotential increased by 351 mV *vs.* Pt/C's 419 mV over the 24 hours time period. The initial rapid decrease is due to the formation of bubbles. Upon replenishing the electrolyte solution (KOH) and removing the bubbles after 24 hours, the actual drop was only 119 mV. The NAC heterostructure's surface is heavily influenced by the method of preparation as directed by the EDL. The core–shell structure with the metallic composite of Pt and the metal oxide–hydroxide layer is obtained due to the EDL of AuNPs which directs the assembly process and the formation of the final catalyst structure. This enhances the surface availability of the elements increasing the atomic utilization of expensive Pt. In combination with the multitude of coordination sites owing to the presence of both metallic and amorphous composite regions and their interfaces, it creates an abundance of unique catalytic sites by taking advantage of several synergistic effects to enhance the water splitting process.

Data availability

The data supporting this article have been included as part of the ESI.†

Conflicts of interest

There are no conflicts to declare.

Acknowledgements

V. M. acknowledges financial support from NSERC, Mitacs, CFI and the University of Waterloo. M. O. is thankful for the financial support by the NSERC CGS D scholarship and the Waterloo Institute for Nanotechnology Nano fellowship program. The University of Waterloo's QNFCF facility was used for this work. This infrastructure would not be possible without the significant contributions of CFREF-TQT, CFI, ISED, the Ontario Ministry of Research & Innovation, and Mike & Ophelia Lazaridis; their support is gratefully acknowledged.

References

1 S. Khamgaonkar, M. Okasha and V. Maheshwari, Recent Advances towards Increasing the Pt Utilization Efficiency for Hydrogen Evolution Reaction: A Review, *Inorg. Chem. Front.*, 2023, **10**(23), 6812–6848, DOI: 10.1039/D3QI01656K.

Open Access Article. Published on 27 December 2024. Downloaded on 2/2/2026 12:09:34 PM. This article is licensed under a Creative Commons Attribution-NonCommercial 3.0 Unported Licence.

2 E. P. George, D. Raabe and R. O. Ritchie, High-Entropy Alloys, *Nat. Rev. Mater.*, 2019, **4**(8), 515–534, DOI: **10.1038/s41578-019-0121-4**.

3 S. A. Lee, J. Bu, J. Lee and H. W. Jang, High-Entropy Nanomaterials for Advanced Electrocatalysis, *Small Sci.*, 2023, **3**(5), 2200109, DOI: **10.1002/SMSC.202200109**.

4 Z. Zhang, J. Hu, B. Li, Q. Qi, Y. Zhang, J. Chen, P. Dong, C. Zhang, Y. Zhang and M. K. H. Leung, Recent Research Progress on High-Entropy Alloys as Electrocatalytic Materials, *J. Alloys Compd.*, 2022, **918**, 165585, DOI: **10.1016/J.JALLCOM.2022.165585**.

5 D. Wu, K. Kusada, T. Yamamoto, T. Toriyama, S. Matsumura, I. Gueye, O. Seo, J. Kim, S. Hiroi, O. Sakata, S. Kawaguchi, Y. Kubota and H. Kitagawa, On the Electronic Structure and Hydrogen Evolution Reaction Activity of Platinum Group Metal-Based High-Entropy-Alloy Nanoparticles, *Chem. Sci.*, 2020, **11**(47), 12731–12736, DOI: **10.1039/D0SC02351E**.

6 X. Huo, H. Yu, B. Xing, X. Zuo and N. Zhang, Review of High Entropy Alloys Electrocatalysts for Hydrogen Evolution, Oxygen Evolution, and Oxygen Reduction Reaction, *Chem. Rec.*, 2022, **22**(12), e202200175, DOI: **10.1002/TCR.202200175**.

7 W. Kucza, High Entropy Alloys and Thermodynamically Derived High Stability Alloys; a Compositional Comparative Study of All 3–7 Element Systems Composed of Ten 3d Metals at 1273 K, *J. Alloys Compd.*, 2022, **894**, 162443, DOI: **10.1016/J.JALLCOM.2021.162443**.

8 S. Wang, A. Lu and C. J. Zhong, Hydrogen Production from Water Electrolysis: Role of Catalysts, *Nano Convergence*, 2021, **8**(1), 1–23, DOI: **10.1186/S40580-021-00254-X/FIGURES/16**.

9 F. Lehner and D. Hart, The Importance of Water Electrolysis for Our Future Energy System. *Electrochemical Power Sources: Fundamentals, Systems, and Applications Hydrogen Production by Water Electrolysis*, 2022, pp. 1–36, DOI: **10.1016/B978-0-12-819424-9.00008-2**.

10 A. L. Maulana, P. C. Chen, Z. Shi, Y. Yang, C. Lizandara-Pueyo, F. Seeler, H. D. Abruña, D. Muller, K. Schierle-Arndt and P. Yang, Understanding the Structural Evolution of IrFeCoNiCu High-Entropy Alloy Nanoparticles under the Acidic Oxygen Evolution Reaction, *Nano Lett.*, 2023, **23**(14), 6637–6644, DOI: **10.1021/ACS.NANOLETT.3C01831/SUPPL_FILE/NL3C01831_SI_001.PDF**.

11 Y. Zhang, J. Kang, H. Xie, H. Yin, Z. Zhang, E. Liu, L. Ma, B. Chen, J. Sha, L. Qian, W. Hu, C. He and N. Zhao, Boosting the Oxygen Evolution of High-Entropy (Oxy)Hydroxide Epitaxially Grown on High Entropy Alloy by Lattice Oxygen Activation, *Appl. Catal., B*, 2024, **341**, 123331, DOI: **10.1016/J.APCATB.2023.123331**.

12 O. Vozniuk, N. Tanchoux, J. M. Millet, S. Albonetti, F. Di Renzo and F. Cavani, Spinel Mixed Oxides for Chemical-Loop Reforming: From Solid State to Potential Application, *Stud. Surf. Sci. Catal.*, 2019, **178**, 281–302, DOI: **10.1016/B978-0-444-64127-4.00014-8**.

13 Z. Cui, W. Jiao, Z. Y. Huang, G. Chen, B. Zhang, Y. Han and W. Huang, Design and Synthesis of Noble Metal-Based Alloy Electrocatalysts and Their Application in Hydrogen Evolution Reaction, *Small*, 2023, **19**(35), 2301465, DOI: **10.1002/SMLL.202301465**.

14 J. Shen, Z. Hu, K. Chen, C. Chen, Y. Zhu and C. Li, Platinum Based High Entropy Alloy Oxygen Reduction Electrocatalysts for Proton Exchange Membrane Fuel Cells, *Mater. Today Nano*, 2023, **21**, 100282, DOI: **10.1016/J.MTNANO.2022.100282**.

15 O. Iqbal, H. Ali, N. Li, A. I. Al-Sulami, K. F. Alshammari, H. S. M. Abd-Rabboh, Y. Al-Hadeethi, I. U. Din, A. I. Alharthi, R. Altamimi, A. Zada, Z. Wang, A. Hayat and M. Zahid Ansari, A Review on the Synthesis, Properties, and Characterizations of Graphitic Carbon Nitride (g-C3N4) for Energy Conversion and Storage Applications, *Mater. Today Phys.*, 2023, 34, DOI: **10.1016/j.mtphys.2023.101080**.

16 H. Bian, P. Qi, G. Xie, X. Liu, Y. Zeng, D. Zhang and P. Wang, HEA-NiFeCuCoCe/NF through Ultra-Fast Electrochemical Self-Reconstruction with High Catalytic Activity and Corrosion Resistance for Seawater Electrolysis, *Chem. Eng. J.*, 2023, **477**, 147286, DOI: **10.1016/J.CEJ.2023.147286**.

17 H. J. Qiu, G. Fang, J. Gao, Y. Wen, J. Lv, H. Li, G. Xie, X. Liu and S. Sun, Noble Metal-Free Nanoporous High-Entropy Alloys as Highly Efficient Electrocatalysts for Oxygen Evolution Reaction, *ACS Mater. Lett.*, 2019, **1**(5), 526–533, DOI: **10.1021/ACSMATERIALSLETT.9B00414/SUPPL_FILE/TZ9B00414_SI_001.PDF**.

18 W. Dai, T. Lu and Y. Pan, Novel and Promising Electrocatalyst for Oxygen Evolution Reaction Based on MnFeCoNi High Entropy Alloy, *J. Power Sources*, 2019, **430**, 104–111, DOI: **10.1016/J.JPOWSOUR.2019.05.030**.

19 L. Pu, H. Fan and V. Maheshwari, Formation of Microns Long Thin Wire Networks with a Controlled Spatial Distribution of Elements, *Catal. Sci. Technol.*, 2020, **10**(7), 2020–2028, DOI: **10.1039/c9cy02365h**.

20 H. Fan and V. Maheshwari, Controlled Element Specific Nanoscale Domains by Self-Assembly for High Performance Bifunctional Alkaline Water Splitting Catalyst, *Adv. Funct. Mater.*, 2021, **31**(46), 2106149, DOI: **10.1002/adfm.202106149**.

21 W. Wang, X. Ding, Q. Xu, J. Wang, L. Wang and X. Lou, Zeta-Potential Data Reliability of Gold Nanoparticle Biomolecular Conjugates and Its Application in Sensitive Quantification of Surface Absorbed Protein, *Colloids Surf., B*, 2016, **148**, 541–548, DOI: **10.1016/j.colsurfb.2016.09.021**.

22 W. J. Zeng, C. Wang, Q. Q. Yan, P. Yin, L. Tong and H. W. Liang, Phase Diagrams Guide Synthesis of Highly Ordered Intermetallic Electrocatalysts: Separating Alloying and Ordering Stages, *Nat. Commun.*, 2022, **13**(1), 7654, DOI: **10.1038/s41467-022-35457-1**.

23 H. Okamoto, Ni–Pt (Nickel–Platinum), *J. Phase Equilib. Diffus.*, 2010, **31**(3), 322, DOI: **10.1007/s11669-010-9701-0**.

24 H. Y. Kim, T. Kwon, Y. Ha, M. Jun, H. Baik, H. Y. Jeong, H. Kim, K. Lee and S. H. Joo, Intermetallic PtCu Nanoframes as Efficient Oxygen Reduction Electrocatalysts, *Nano Lett.*, 2020, **20**(10), 7413–7421, DOI: **10.1021/acs.nanolett.0c02812**.

25 L. Bu, N. Zhang, S. Guo, X. Zhang, J. Li, J. Yao, T. Wu, G. Lu, J.-Y. Ma, D. Su and X. Huang, Biaxially Strained PtPb/Pt Core/Shell Nanoplate Boosts Oxygen Reduction Catalysis, *Science*, 2016, **354**(6318), 1410–1414, DOI: **10.1126/science.aah6133**.

26 T. He, W. Wang, F. Shi, X. Yang, X. Li, J. Wu, Y. Yin and M. Jin, Mastering the Surface Strain of Platinum Catalysts for Efficient Electrocatalysis, *Nature*, 2021, **598**(7879), 76–81, DOI: **10.1038/s41586-021-03870-z**.

© 2025 The Author(s). Published by the Royal Society of Chemistry

Open Access Article. Published on 27 December 2024. Downloaded on 2/2/2026 12:09:34 PM.
This article is licensed under a Creative Commons Attribution-NonCommercial 3.0 Unported Licence.

27 C. Zhan, H. Sun, L. Lü, L. Bu, L. Li, Y. Liu, T. Yang, W. Liu and X. Huang, Zinc Intercalated Lattice Expansion of Ultrafine Platinum–Nickel Oxygen Reduction Catalyst for PEMFC, *Adv. Funct. Mater.*, 2023, **33**(8), 2212442, DOI: 10.1002/adfm.202212442.

28 Q. Chen, B. Wei, Y. Wei, P. Zhai, W. Liu, X. Gu, Z. Yang, J. Zuo, R. Zhang and Y. Gong, Synergistic Effect in Ultrafine PtNiP Nanowires for Highly Efficient Electrochemical Hydrogen Evolution in Alkaline Electrolyte, *Appl. Catal., B*, 2022, **301**, 120754, DOI: 10.1016/J.APCATB.2021.120754.

29 P. Gono and A. Pasquarello, High-Performance NiOOH/FeOOH Electrode for OER Catalysis, *J. Chem. Phys.*, 2021, **154**(2), 024706, DOI: 10.1063/5.0036019/200160.

30 T. S. Amarnath, S. Chatterjee, K. Karthick and S. Kundu, Respective Influence of Stoichiometry and NiOOH Formation in Hydrogen and Oxygen Evolution Reactions of Nickel Selenides, *Appl. Surf. Sci.*, 2019, **487**, 1152–1158, DOI: 10.1016/J.APSUSC.2019.05.118.

31 D. Rathore, A. Banerjee and S. Pande, Bifunctional Tungsten-Doped Ni(OH)2/NiOOH Nanosheets for Overall Water Splitting in an Alkaline Medium, *ACS Appl. Nano Mater.*, 2022, **5**(2), 2664–2677, DOI: 10.1021/ACSANM.1C04359/ASSET/IMAGES/LARGE/AN1C04359_0010.JPEG.

32 S. Yan, K. P. Abhilash, L. Tang, M. Yang, Y. Ma, Q. Xia, Q. Guo and H. Xia, Research Advances of Amorphous Metal Oxides in Electrochemical Energy Storage and Conversion, *Small*, 2019, **15**(4), 1804371, DOI: 10.1002/SMLL.201804371.

33 Y. Zhou and H. J. Fan, Progress and Challenge of Amorphous Catalysts for Electrochemical Water Splitting, *ACS Mater. Lett.*, 2021, **3**(1), 136–147, DOI: 10.1021/ACSMATERIALSLETT.0C00502/ASSET/IMAGES/MEDIUM/TZ0C00502_0010.GIF.

34 J. C. Qiao, Q. Wang, J. M. Pelletier, H. Kato, R. Casalini, D. Crespo, E. Pineda, Y. Yao and Y. Yang, Structural Heterogeneities and Mechanical Behavior of Amorphous Alloys, *Prog. Mater. Sci.*, 2019, **104**, 250–329, DOI: 10.1016/J.PMATSCI.2019.04.005.

35 J. Park, S. Lee and S. Kim, Recent Advances in Amorphous Electrocatalysts for Oxygen Evolution Reaction, *Front. Chem.*, 2022, **10**, 1030803, DOI: 10.3389/FCHEM.2022.1030803/BIBTEX.

36 Z. Cui and R. Qi, First-Principles Simulation of Oxygen Evolution Reaction (OER) Catalytic Performance of IrO_2 Bulk-like Structures: Nanosphere, Nanowire and Nanotube, *Appl. Surf. Sci.*, 2021, **554**, 149591, DOI: 10.1016/J.APSUSC.2021.149591.

37 Z. Cao, F. Dong, J. Pan, W. Xia, J. G. Hu and X. Xu, Heteroatomic Platinum-Cobalt Synergetic Active Centers with Charge Polarization Enable Superior Hydrogen Evolution Performance in Both Acid and Base Media, *ACS Appl. Energy Mater.*, 2022, **5**(2), 1496–1504, DOI: 10.1021/ACSAEM.1C02877/SUPPL_FILE/AE1C02877_SI_003.MP4.

38 T. Shinagawa, A. Garcia-Esparza and K. Takanabe, Insight on Tafel slopes from a microkinetic analysis of aqueous electrocatalysis for energy conversion, *Sci. Rep.*, 2015, **5**, 13801, DOI: 10.1038/srep13801.

39 H. Chen, C. Guan and H. Feng, Pt-Based High-Entropy Alloy Nanoparticles as Bifunctional Electrocatalysts for Hydrogen and Oxygen Evolution, *ACS Appl. Nano Mater.*, 2022, **5**(7), 9810–9817, DOI: 10.1021/ACSANM.2C02003/SUPPL_FILE/AN2C02003_SI_001.PDF.

40 I. T. McCrum and M. T. M. Koper, The Role of Adsorbed Hydroxide in Hydrogen Evolution Reaction Kinetics on Modified Platinum, *Nat. Energy*, 2020, **5**(11), 891–899, DOI: 10.1038/s41560-020-00710-8.

© 2025 The Author(s). Published by the Royal Society of Chemistry